Journal of Dynamic Behavior of Materials (2022) 8:405–417
https://doi.org/10.1007/s40870-022-00344-9

RESEARCH PAPER

Energy Dissipation Pathway Control in Polymer Derived Ceramic (PDC) Composites

Y. Li[1] · C. Ma[1] · K. Larkin[1]

Received: 18 January 2022 / Accepted: 7 June 2022 / Published online: 1 July 2022

Abstract

Ceramics are brittle due in large part to the limited availability of energy dissipation pathways when they are subjected to an impact load. The primary avenue for improving the material reliability and energy-absorption capability is to create new energy dissipation mechanisms that can be used to replace or minimize the kinetic energy associated with the debris shattering. In this paper, a computational framework is developed to investigate the relationship between phase composition and energy dissipation pathways in polymer derived ceramic (PDC) composites by accounting for the key processing parameters and deformation/failure mechanisms. It is found that the phase composition that promotes both the Mullins effect and the ligament bridging mechanism can significantly improve the structural integrity of the composite material. A fundamental understanding of how to redistribute the impact energy dissipation in a controllable path would hold great promise for fabricating PDC composites with tailored properties.

Keywords Energy pathway analysis · Polymer-derived ceramic (PDC) composites · Impact simulation · Phase transition analysis

Introduction

The route of devising polymer-derived ceramics (PDCs), which relies on heat treatment to convert preceramic polymers to ceramics, presents a flexible and energy-efficient approach to fabricate a broad spectrum of ceramics and in-situ ceramic-polymer composites with binary or multinary phases [1]. Understanding the relationship among processing parameters, phase composition and material response holds an important key for property tailoring of PDC composites in different engineering applications.

Brittleness and low reliability are the foremost drawbacks of conventional ceramics. This is primarily due to the fact that slip systems in pure ceramics are limited and difficult to activate [2]. Therefore, energy tends to dissipate through fracture formation or even debris shattering when plastic deformation is negligible. This type of energy dissipation pathway leads to sudden brittle fracture and low structure integrity in monolithic ceramics. Inclusion of a polymer phase in ceramics can change the energy dissipation pathway by creating new dissipation mechanisms, such as plastic and viscous deformation, which barely exist in pure ceramics. Osnes et al. [3] compared the fracture behavior in monolithic glass plates and laminated glass plates with polyvinyl butural (PVB) interlayer. Both the experiment and simulation results demonstrate that the polymer interlayer can effectively retain broken glass fragments and increase the material energy absorption capability. Deformation of the PVB interlayer absorbs energy and in turn reduces the energy transmitted to the rest of the structure. Yadav and Ravichandran [4] also proved that the penetration resistance of laminated ceramic-polymer structures is significantly higher than that of monolithic ceramic structures of the same total thickness. Tan et al. [5] found that a bioinspired nacre-like zirconia-PMMA composite demonstrate a staircase-like fracture behavior under cyclic compression. Transition in failure mode from the fracture of ceramic bricks to separation along the inter-brick polymer phase leads to improved fatigue resistance and better structural integrity. Grujicic et al. [6] also pointed out that the hierarchical microstructure in ceramic-polymer laminated composite plays a critical role in failure/deformation behaviors. Compared to fabricating ceramic-polymer composites through lamination, polymer-derived ceramics

✉ Y. Li
yan.li@dartmouth.edu

[1] Thayer School of Engineering, Dartmouth College, Hanover, NH 03755, USA

route can directly yield in-situ hybrid/gradient ceramic-polymer composites through pyrolysis control. Recent advancements in additive manufacturing [7–9] also pave the way for tool-less and net-shape fabrication of PDC composites with complex microstructure/structure architectures that are impossible to make via other processing techniques. However, the poor linkage among process physics, microstructure, material response, and key processing parameters have limited our ability to tailor properties of PDC composites to the level of trial and error.

In this paper, a computational framework is developed to understand the correlation between phase composition and energy dissipation pathways by accounting for the key processing parameters and deformation/failure mechanisms. Calculations in this work concern PDC composites that are pyrolyzed from polymethylhydrosiloxane (PMHS) crosslinked by divinylbenzene (DVB). Coupled heat transfer and phase transition simulations are carried out first on PMHS/DVB samples with varied pyrolysis temperatures in "Phase Composition Prediction" section. The phase composition map of each pyrolyzed sample is extracted and incorporated into a finite element model for impact simulation as discussed in "Impact model description" section. The energy dissipation pathway in each sample configuration is elucidated by finding the link between processing parameters and deformation/failure behaviors as discussed in "Results and Discussion" section. The relations established here can be used for future manufacturing of PDC composites with tailored mechanical properties.

Phase Composition Prediction

Polymer-to-ceramic phase transition is a highly dynamic multiscale and multiphysics event. When the PMHS/DVB precursor is heated up to 150 °C or higher, polymer decomposition occurs [10]. At the atomic level, this process is associated with bond breakage (e.g., Si–H and Si–CH_3) and new bond formation (e.g., H–H and CH_3–H). As a result, gaseous products, such as hydrogen, methane, and other carbon- and hydrogen-containing species can be generated [11]. Ceramic structure starts to form when the gaseous molecules are diffused out of the material [12]. At the continuum level, ceramic phase formation depends on the interplay between gas generation and gas diffusion. According to the conclusions of our earlier work [13], the total amount of gaseous products that can be generated only depends on the pyrolysis temperature. Due to the huge discrepancy of thermal properties in polymers and ceramics, heat transfer in the ceramic phase and intermediate phase is much faster than that in the undecomposed polymer region, leading to non-uniform spatial temperature distribution [14]. Gas diffusion is triggered as a result of a spatial gas density gradient. Ceramic fraction f in the intermediate phase is predicted according to

$$f = \frac{\psi_{\text{release}}}{\psi^{\max}}, \tag{1}$$

where ψ_{release} and $\psi^{\max}$ are the released gas density and the maximum gas density that can be generated in a given element, respectively. The detailed algorithm, which dynamically updates the thermal properties of the intermediate zone by accounting for the real-time temperature field and phase composition change, is discussed in considerable detail in Ma and Li [13]. The developed multiscale framework can be applied to any preceramic polymer systems with arbitrary geometries and heating/cooling histories. In this study, we consider pyrolyzing a set of square PHMS/DVB plates with a thickness of 1 mm, 10 mm and 20 mm, respectively. The side dimension of each plate is 160 mm as illustrated in Fig. 1a. According to the heating–cooling history in Fig. 1b, surface 1 of each plate is heated up from 300 K to 1273 K at that heating rate of 0.61 K/s. After 1600 s, cooling starts at the same rate on surface 1, while surface 2 is kept at 300 K during this process. The same heating–cooling cycle

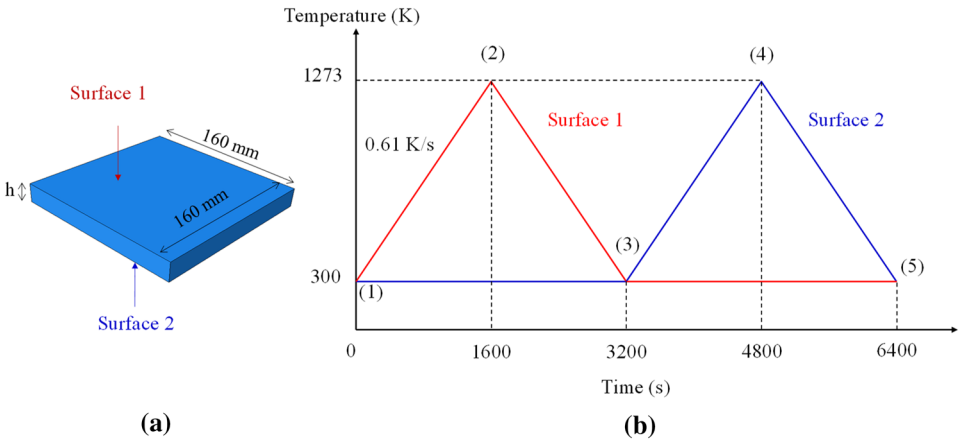

Fig. 1 Scheme of **a** sample configuration and **b** processing history with heating/cooling rate of 0.61 K/s and pyrolysis temperature of 1273 K

is applied to surface 2 at 3200 s while the temperature of surface 1 is kept at 300 K. Figure 2 illustrates the evolution of temperature field and phase composition map in a plate with thickness of 20 mm at five representative stages. It was noticed that only a thin layer of materials at surface 1 and surface 2 had been fully converted to the ceramic phase at $t = 6400$ s. This phase composition map is extracted and implemented in the finite element model in "Impact Model Description" section for impact simulation.

Impact Model Description

Finite Element Model Configuration

3D finite element simulations were carried out in ABAQUS/Explicit to analyze the failure behaviors in a set of pyrolyzed samples. As shown in Fig. 3, all four edges of the square plate were fixed. A rigid ball with a radius of 10 mm impacted the plate with an initial velocity $V = 200$ m/s. Contact between the ball and the plate was modeled according to the kinematic contact algorithm [15]. Adequately refined mesh is required to accurately resolve the stress distribution during the ball-plate interactions. It is sufficient to have the impact load taken place over the span of 10 elements in the thickness direction. The selection of mesh size e in different regions follows:

$$e \le \frac{1}{10} \times t_0 \times C_w, \tag{2}$$

where $t_0 \approx 2 \times 10^{-4}$s is the impact duration, and $C_w = \sqrt{E/\rho}$ is the longitudinal wave speed. The elastic modulus E in each region can be determined from the stress–strain curves

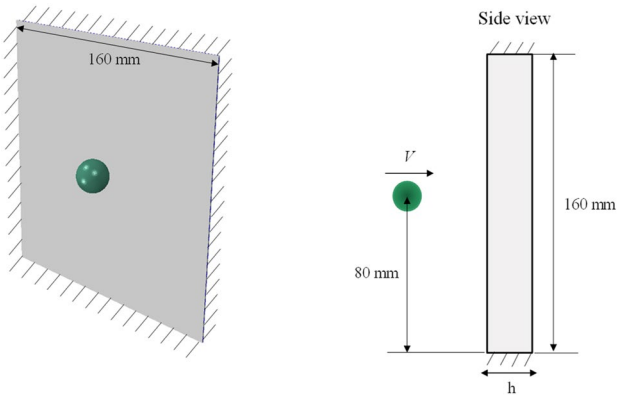

Fig. 3 Scheme of the impact model

as shown in Fig. 4b. The density ρ is calculated according to the ceramic fraction f. In this work, 8-node brick element (C3D8) with size from 0.8 mm to 3 mm is employed in the following simulations.

Constitutive Modeling

Constitutive Behavior of the Preceramic Polymer Phase

When polymers are subjected to simple tension from their virgin state, the stress required for the subsequent reloading after unloading is usually less than that following the initial stress–strain curve until the material reaches the previous maximum stretch. This type of stress softening, which is also referred to as the "Mullins effect" [16, 17], can lead to energy dissipation due to the damage associated with polymer chain disentanglement, chain scission, cross-link breakage, etc. In

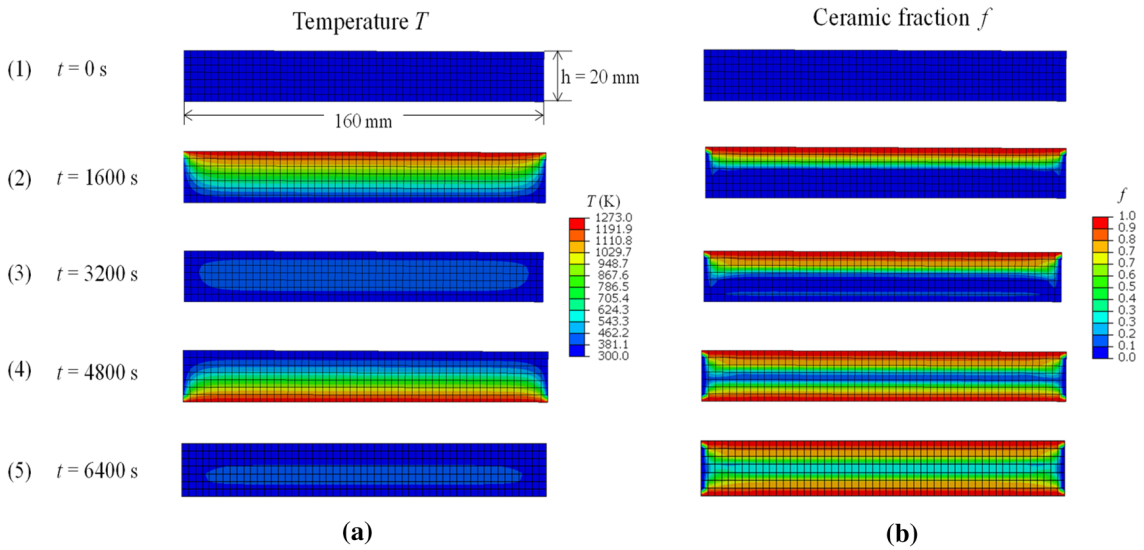

Fig.2 Temperature evolution and corresponding phase transition in a PHMS/DVB square plate with thickness of 20 mm

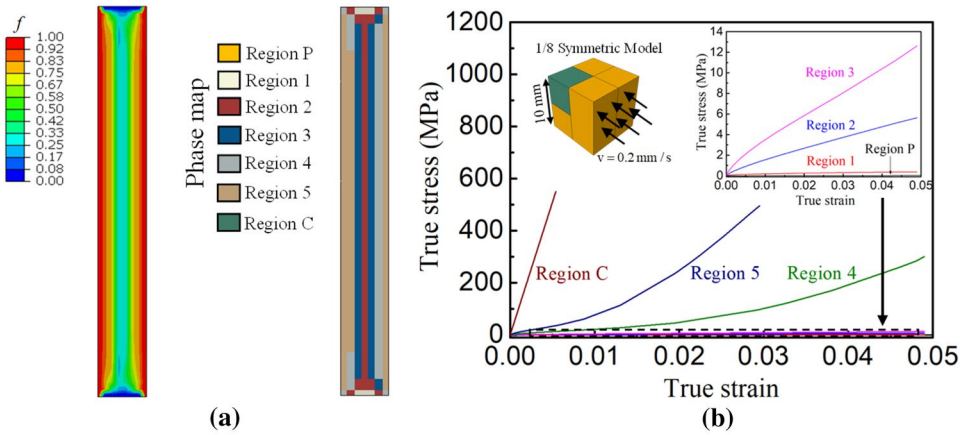

Fig. 4 **a** Illustration of phase distribution in a 20 mm thick sample after complete heating–cooling cycle with maximum temperature of 1273 K under the heating rate of 0.63 K/s; and **b** Stress–strain response in the intermediate regions

Table 1 Constitutive modeling parameters of the preceramic polymer phase [21]

K_1	0.5
K_2	− 0.2
K_3	0.1
m	0.75
p	0.9
q	1.85
D	0.00186495

this work, a modified Yeoh hyperelastic material model [18] is employed to describe the constitutive behavior in the preceramic polymer region.

For hyperelastic polymers without the consideration of the Mullins effect, the strain energy density W can be decomposed as

$$W = W_{dev} + W_{vol}, \tag{3}$$

where W_{dev} and W_{vol} represent the deviatoric and volumetric parts of the strain energy density function, respectively. Their mathematical formations follow

$$\begin{cases} W_{dev} = K_1(I_1 - 3)^m + K_2(I_1 - 3)^p + K_3(I_1 - 3)^q, \text{ and} \\ W_{vol} = 1/D(J-1)^2, \end{cases} \tag{4}$$

where K_1, K_2, K_3, m, p, q, D are the fitting parameters as summarized in Table 1 according to the work of Hanson et al. [19]. I_1 and J are the first stretch invariant and the volumetric ratio, respectively.

When the Mullins effect is considered, the damage energy dissipation upon the initial stretch and stress softening during the subsequent stretches should be accounted for. The revised strain energy density function $\tilde{W}$, which includes the damage dissipation function $\phi(\eta)$ and the damage variable η, is formulated as

$$\tilde{W} = (1-\eta)W_{dev} + \phi(\eta) + W_{vol}. \tag{5}$$

According to Volokh [20], $\phi(\eta)$ and η are expressed in the form of

$$\begin{cases} \phi(\eta) = W_0(\eta + (1-\eta)\ln(1-\eta)), \text{ and} \\ \eta = 1 - \exp(\dfrac{-W_{dev}^m}{W_0}). \end{cases} \tag{6}$$

Here, W_{dev}^m is the maximum deviatoric strain energy density within the previous deformation after unloading, and W_0 is the material failure energy density. For the preceramic polymers considered in this paper, $W_0 \approx 1.12 \times 10^6\,\text{J/m}^3$ [21]. Here, $\eta = 0$ represents the zero deformation state, as $\tilde{W}$ is reduced to W according to eqn. (5). $\eta = 0.63$ corresponds to the maximum stress softening state when $W_{dev}^m = W_0$. The stress is resolved by calculating the first derivative of the corresponding strain energy function with respect to the stretch. Specifically, the deviatoric stress due to the Mullins effect is a rescaling of the deviatoric stress of the primary material response with the damage variable η. The volumetric stress, on the other hand, remains unchanged even if the Mullins effect is taken into account. Fracture in the preceramic polymer phase is modeled according to the maximum tensile strength criterion [14]. Shear failure is not considered here. A VUMAT subroutine was developed to implement the constitutive model.

Constitutive Behavior of the Ceramic Phase

The fully converted ceramic phase follows the isotropic linear elastic constitutive law before failure occurs. The brittle cracking model in Abaqus/Explicit is employed to describe the linear post-failure behavior. In this approach, crack initiation occurs when the maximum principal stress reaches the maximal tensile stress σ_{ts}. Multiple cracks can initiate at a point with crack orientations governed by the principal stress directions. Crack growth is modeled through element

deletion when the scalar stiffness degradation factor equals to 1.

Specifically, the mode I crack growth behavior is determined by the maximum crack displacement δ_{cd} through

$$\delta_{cd} = 2G_f/\sigma_{ts}, \tag{7}$$

where G_f is the fracture energy per unit area. Here, linear stiffness degradation is assumed in the ceramic phase. The shear retention model is employed to simulate the stiffness degradation in mode II fracture. The corresponding post-cracked shear modulus μ_c is defined as

$$\mu_c = \beta\mu_0. \tag{8}$$

Here μ_0=45.5 GPa is the shear modulus of the uncracked material. The shear retention factor β is formulated as [22]

$$\beta = (1 - \frac{\varepsilon_{nn}^{ck}}{\varepsilon_{\max}^{ck}})^{\alpha}, \tag{9}$$

where $\varepsilon_{\mathrm{nn}}^{ck}$ and $\varepsilon_{\max}^{ck}$ represent the current crack opening strain and the maximum crack opening strain, respectively. All the modeling parameters of the ceramic phase are summarized in Table 2.

Constitutive Behavior of the Intermediate Phase

In the intermediate region where the material has started polymer decomposition but has not yet reached the fully ceramic state, the constitutive relationship is not available in the existing literature. In this study, five representative intermediate regions are selected according to the range of ceramic fraction f as summarized in Table 3. The ultimate strength of region i ($1 \le i \le 5$) is estimated according to

$$\sigma_{\mathrm{ts\_i}} = f_i\sigma_{\mathrm{ts\_c}} + (1 - f_i)\sigma_{\mathrm{ts\_p}}. \tag{10}$$

Here $\sigma_{\mathrm{ts\_c}}$ = 550 MPa [24] and $\sigma_{\mathrm{ts\_p}}$ = 1.5 MPa[14] are the tensile strengths of pure ceramic phase and pure polymer phase, respectively. f_i is the averaged ceramic fraction in region i. In each region, the stress–strain relationship before reaching the ultimate strength is determined from the simple compression simulation as shown in Fig. 4b. 1/8 symmetric model is employed to improve the computational efficiency. The calculated stress–strain response in each region, as shown in Fig. 4b, is imported to ABAQUS for material property assignment.

Table 2 Constitutive modeling parameters of the ceramic phase

Density ρ [23]	2230 kg/m^3
Elastic modulus E [23]	101 GPa
Poisson's ratio ν [23]	0.11
Maximal tensile stress σ_{ts} [24]	550 MPa
Fracture energy G_f [25]	5.36 N/m
Maximum crack opening strain $\varepsilon_{\max}^{ck}$[22]	5e^{-5}
α[26]	2

Table 3 Domain decomposition criterion

Different regions	Ceramic fraction
Region P	$f = 0$
Region 1	$0 < f \le 20\%$
Region 2	$20 < f \le 40\%$
Region 3	$40 < f \le 60\%$
Region 4	$60 < f \le 80\%$
Region 5	$80 < f \le 100\%$
Region C	f=100%

Energy Pathway Analysis

During the ball-plate interactions, the mechanical energy is primarily dissipated in two modes: energy transfer and energy absorption. Energy transfer consists of elastic strain energy and kinetic energy, which are transferred back to the ball or the environment through vibration and damping. Energy absorption, on the other hand, includes permanent inelastic deformation and damage-induced fracture energy. As shown in Fig. 5, the velocity of the ball starts to decrease when it hits the plate. If friction is ignored, the kinetic energy of the ball will be fully transferred to the plate and stored as the elastic strain energy when no damage or permanent deformation occurs. When the ball speed decreases to 0, the maximum elastic strain energy of the plate is reached. The subsequent rebound is accompanied by the recovery of the elastic strain in the plate. This ideal case scenario is not applicable to this study as both damage and inelastic deformation are associated with the collision process. Ball penetration would occur if the kinetic energy of the rigid ball exceeds the maximum strain energy that can be accommodated by the plate before damage initiation. Prediction of the actual interaction mode, as well as the fracture behavior of the PDC composite plate requires calculation of the following energy paths: kinetic energy of the ball ($E_K^b = \frac{1}{2}m_b v_b^2$,where m_b is the ball mass and v_b is the ball velocity), kinetic energy of the plate ($E_K^p = \frac{1}{2}\int_{m_p} v_p^2 dm_p$, where m_p is the plate mass and v_p is the plate velocity), strain energy of the plate ($E_S^p = \int_{V_p} \boldsymbol{\sigma} : \boldsymbol{\varepsilon} dV_p$, where $\boldsymbol{\sigma}$ is the stress

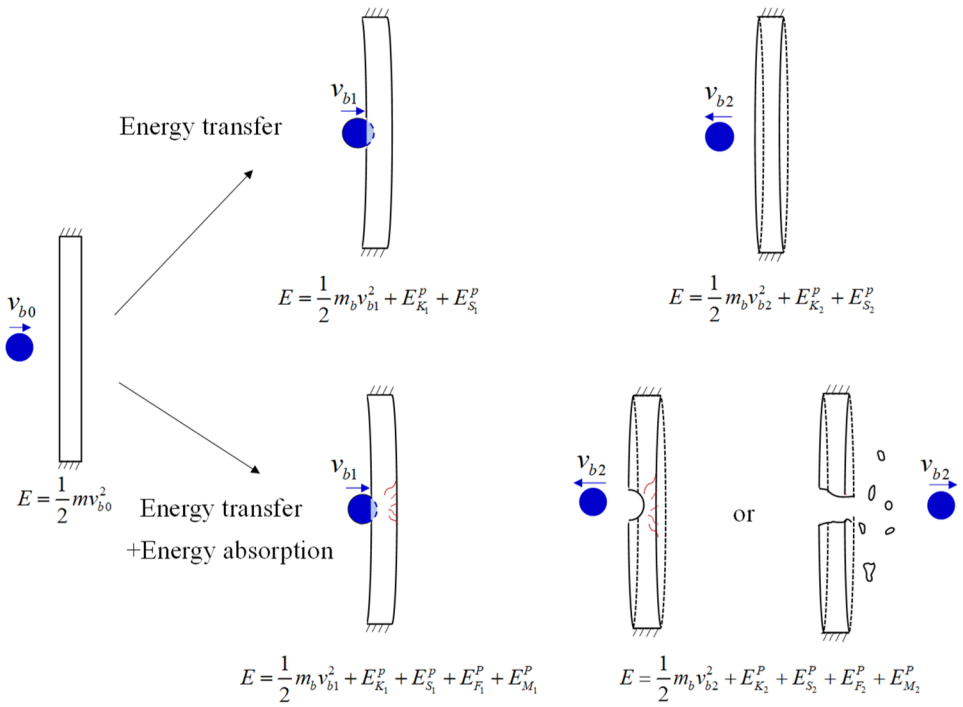

Fig. 5 Scheme of energy dissipation pathways during the ball-plate interactions

and ε is the strain in the plate), energy dissipation via the Mullins effect ($E_M^p = \int_{V_p} \phi(\eta) dV_p$, where $\phi(\eta)$ is Mullins damage energy density); the fracture energy dissipation of the plate ($E_F^p = \int_A G dA$, where G is the fracture energy per unit crack area and A is the crack area). The detailed energy dissipation pathways in different PDC compositions and their relationships with mechanical response and processing parameters are discussed in "Results and Discussion" section.

Results and Discussion

Both idealized and gradient samples are employed for energy pathway calculation and failure analysis. Three sets of idealized samples with thickness of 1 mm, 10 mm and 20 mm are listed in Fig. 6, respectively. Each set includes a preceramic polymer sample, a ceramic-polymer composite sample, and a fully converted ceramic sample. Figure 7 illustrates four gradient PDC composite samples, which are pyrolyzed at 873 K, 1073 K, 1273 K and 1673 K,

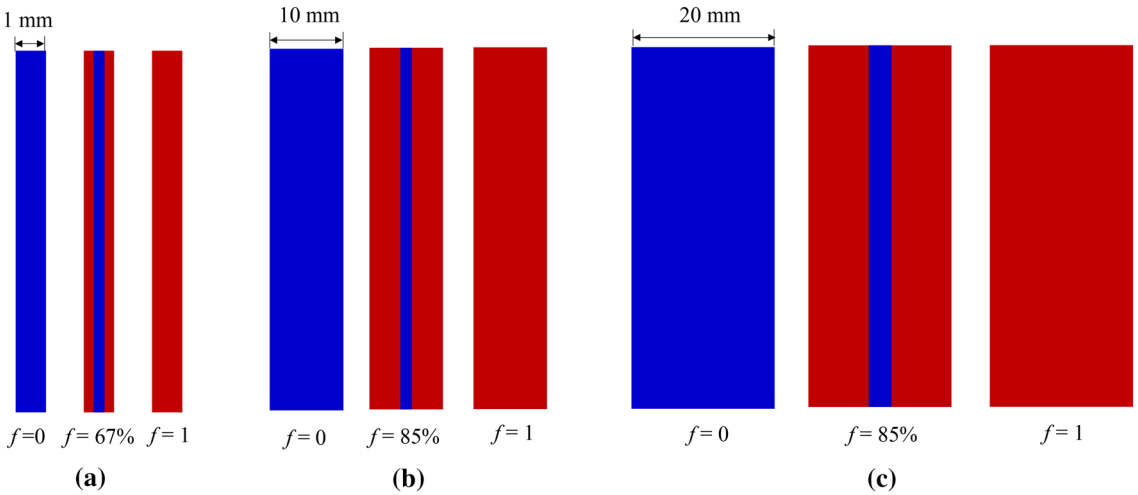

Fig. 6 Scheme of the idealized samples with thickness of **a** 1 mm, **b** 10 mm, and **c** 20 mm, respectively

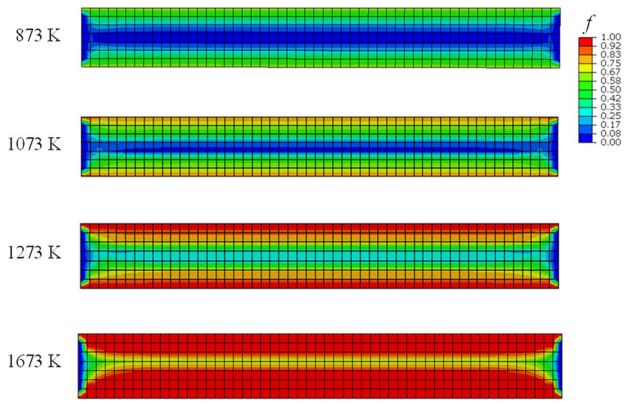

Fig. 7 Phase composition of 20 mm gradient samples under different maximum pyrolysis temperatures

respectively. The pyrolysis follows the heating–cooling history as shown in Fig. 1b.

Effect of Phase Composition on Energy Dissipation Pathways

Energy pathway calculations are first carried out on idealized samples with thickness of 1 mm as shown in Fig. 6a. In a fully converted ceramic sample, an abrupt increase of kinetic energy is observed at 6×10^{-5} s, according to Figs. 8a and 9a. This moment, which also corresponds to an 80.3% decrease in the stored strain energy, signifies the onset of debris shattering. This type of energy redistribution is a manifestation of brittle response in the pure ceramic plate. The abrupt kinetic energy increase is not observed in the pure polymer plate within the same period of time as the ball has not gone through the plate yet. The polymer plate keeps being stretched in the thickness direction with a linear increase in the strain energy as indicated in Fig. 9b. It can be seen from Figs. 8c and 9c that a symmetric ceramic-polymer composite sample with a ceramic fraction of 67% can slightly postpone the ball penetration. This sample composition also leads to a greater amount of absorbed strain energy compared to that of the pure ceramic plate. Most importantly, inclusion of the polymer phase can significantly alleviate debris shattering as shown in Fig. 8c. The reason is several-fold. Firstly, crack propagation in a pure ceramic plate tends to be localized, as the fracture-impacted area is only slightly larger than the ball according to Fig. 8a. In contrast, a much larger fracture-impacted area is observed in the ceramic-polymer composite sample, leading to higher fracture energy dissipation. As illustrated in Fig. 8c, crack branching along the radial direction is quite prominent in addition to the crack propagation in the circumferential direction. It is noted that this fracture pattern includes many uncracked ligaments, which bridge the radial cracks and circumferential cracks. This toughening

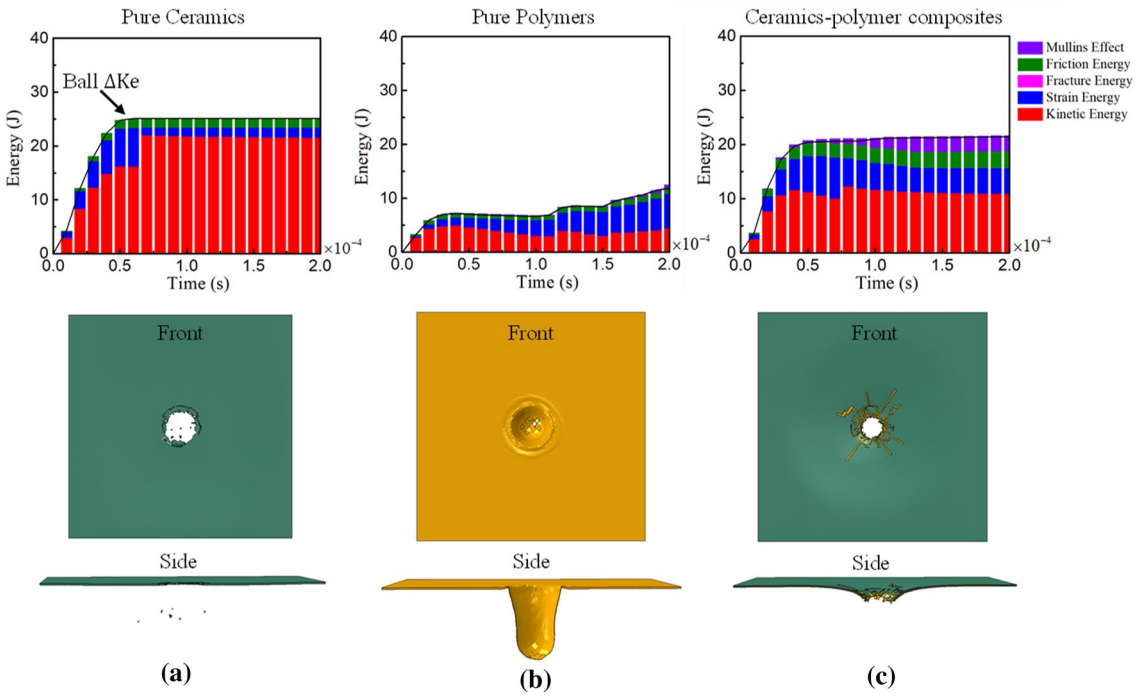

Fig. 8 Energy pathway analysis and failure mode in **a** pure ceramics, **b** pure polymers, and **c** ceramic-polymer composites. Plate thickness is 1 mm

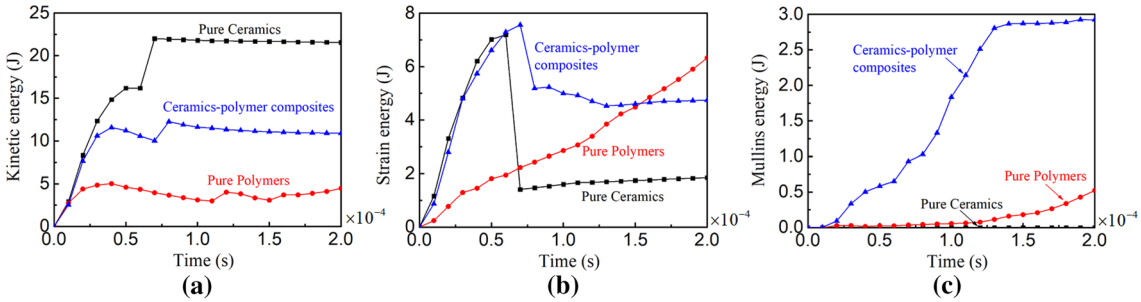

Fig. 9 Comparison of **a** kinetic energy, **b** strain energy and **c** Mullins effect associated energy distribution in samples in Fig. 6a

mechanism allows the material to continue absorbing additional strain energy without immediately losing its load bearing capacity. Additionally, the enlarged damage zone in the ceramic-polymer composite sample not only promotes greater fracture energy dissipation, but also results in more pronounced energy dissipation due to the Mullins effect. This is because the ceramic-polymer composites can experience multiple loading–unloading cycles during the ball-plate interactions. First, microcrack initiation leads to local material unloading. Due to the ligament bridging effect, the adjacent regions can continue to carry load before further damage progression is reached. The irreversible energy dissipation due to stress softening and fracture surface creation can effectively accommodate the kinetic energy that is allocated for debris shattering in the pure ceramics. The redistributed energy pathways ultimately lead to improved material integrity and energy absorption capability in the ceramic-polymer composites.

Effect of Plate Thickness and Ceramic Fraction on Energy Dissipation Pathways

Results from "Effect of Phase Composition on Energy Dissipation Pathways" section indicate that lamination of a polymer layer in the middle of a 1 mm ceramic plate can lead to higher strain energy absorption and better material integrity. In this section, the roles of plate thickness and ceramic fraction on material response and energy dissipation pathways are quantitatively studied. In the first set of study, we consider 1 mm plates with ceramic fraction f of 33%, 67%, 90% and 100%, respectively. We find similar trends as discussed in "Effect of Phase Composition on Energy Dissipation Pathways" section. Decreasing f from 100 to 33% can postpone the ball penetration time from 6×10^{-5} s to 8×10^{-5} s. The moment of ball penetration corresponds to the sudden increase in kinetic energy (Fig. 10a) and abrupt decrease in strain energy (Fig. 10b). It is interesting to notice that increasing f also leads to earlier saturation of the Mullins energy and a lower plateau value. The Mullins effect completely disappears when f reaches 100%. Although the sample with $f = 33\%$ yields the highest plateau value, its initial Mullins energy dissipation is even lower than the samples with $f = 67\%$ and 90% as shown in Fig. 10c. This is because the Mullins energy dissipation requires repetitive loading/unloading cycles that are triggered by the crack growth and vibration. Prior to the ball penetration at 8×10^{-5} s, the 33% sample is in the pure "stretching" mode with negligible damage-induced unloading behavior. When ball penetration occurs, its Mullins energy quickly picks up as cracks start to grow in both radial and circumferential directions. As illustrated in Fig. 11, the 33% sample has

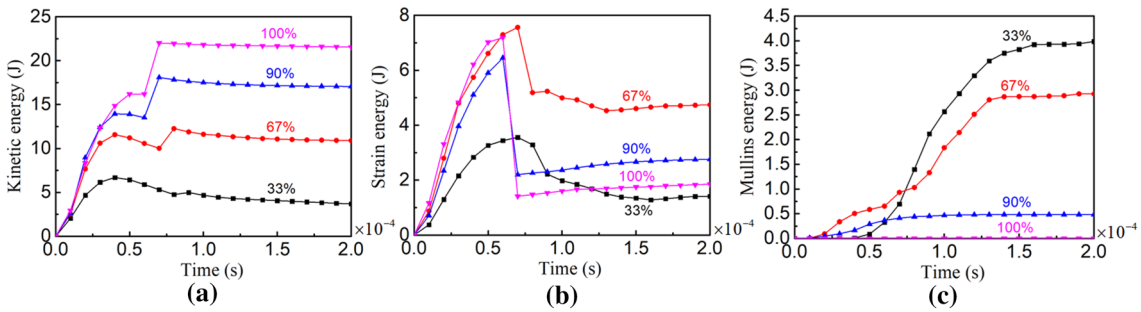

Fig. 10 Effect of ceramic fraction f on **a** kinetic energy, **b** strain energy and **c** Mullins effect associated energy distribution in 1 mm thickness samples. Here $f = 33\%,\ 67\%$, 90% and 100%, respectively

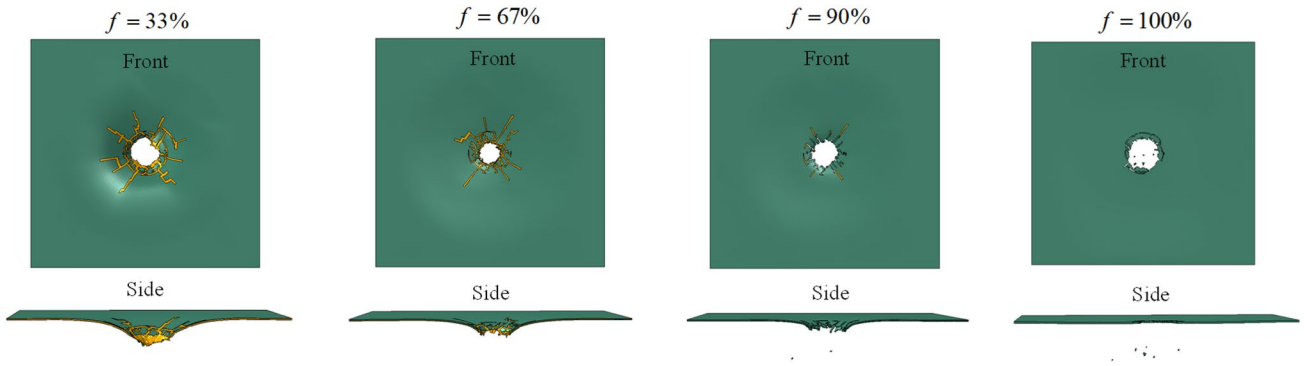

Fig. 11 Effect of ceramic fraction f on fracture patterns. The sample thickness is 1 mm

the largest fracture zone with the longest radial cracks. Therefore, a larger portion of the material can engage in the loading/unloading cycles, leading to more pronounced Mullins effect. According to our analysis, a 1 mm composite plate with $f = 33\%$ and 67% can effectively eliminate debris shattering by converting the kinetic energy into fracture energy and Mullins energy. However, it should be noted that the 33% sample exhibits the lowest strain energy after ball penetration. This indicates that there is a trade-off between the structural integrity and load bearing capacity. Decreasing the ceramic fraction from 67 to 33% does not help much with the structural integrity. But it can significantly jeopardize the load bearing capacity as the strength in ceramic phase is almost 367 times than that in the polymer phase. In this set of study, the sample with $f = 67\%$ exhibits the most balanced load-bearing capacity and structural integrity.

In the second set of study, energy density is employed due to the change of sample volume when the thickness varies. According to Fig. 12a, a sudden increase in kinetic energy density is observed in all the pure ceramic plates regardless of the thickness. The increase of plate thickness from 1 to 20 mm, although postponing the time for ball penetration from 0.7×10^{-4} s to 1.4×10^{-4} s, does not change the brittle response because the remaining strain energy densities after the sudden drop are all kept at low levels, as indicated in

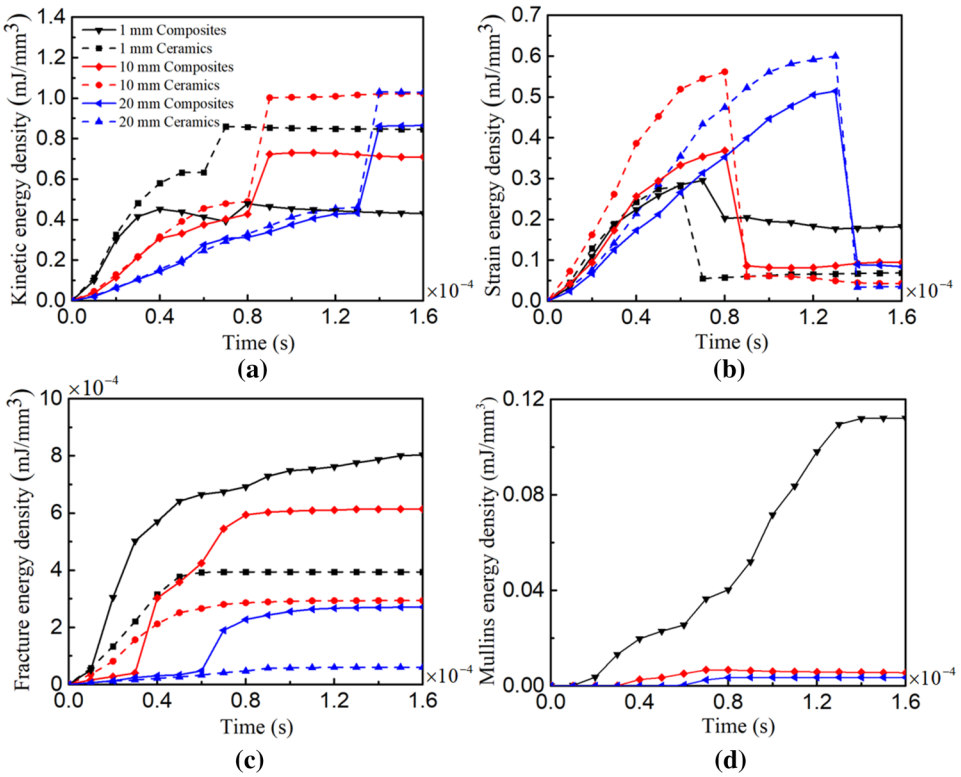

Fig. 12 Comparison of **a** kinetic energy density, **b** strain energy density, **c** fracture energy density, and **d** Mullins damage density in plates with varying thickness and ceramic volume fraction. Solid and dashed lines represent composite and pure ceramics, respectively

Fig. 12b. When the ceramic fraction is reduced to 85% in the 10 mm and 20 mm composite plates, lower magnitudes of kinetic energy increases are observed compared to their pure ceramic counterparts. Further decrease of ceramic fraction to 67% in the 1 mm composite plate can significantly alleviate the kinetic energy jump, while maintaining almost four times higher strain energy density than the rest of the cases as shown in Fig. 12a. Additionally, the corresponding energy dissipations due to fracture surface formation and Mullins effect are the highest in the 1 mm composite sample as illustrated in Fig. 12c, d. The above calculations indicate that the kinetic energy redistribution only occurs in a limited ceramic region that is adjacent to the polymer phase. The ligament bridging mechanism, which improves material strength and integrity by gluing the fractured ceramic pieces without scattering, becomes less effective in the ceramic regions that are not in direct contact with the polymer phase. This can be seen from Fig. 13b that the 20 mm composite plate exhibits the most extensive debris shattering when ball penetration occurs. Apparently, the polymer phase is unable to keep all the fracture pieces in place as it did in the 1 mm sample. Reducing the composite plate thickness from 20 to 10 mm while keeping the same ceramic fraction does not significantly promote the Mullin's effect related energy dissipation. This is because the fracture pattern is still localized without noticeable radial crack branching as observed in Fig. 13a.

It can be inferred from the above discussion that replacing the pure ceramic phase with a gradient polymer-to-ceramic phase may improve the energy absorption and structural integrity of a thick composite plate. The unique polymer-to-ceramic phase transition in PDCs allows fabrication of a broad spectrum of ceramic-polymer composites with controllable phase composition and mechanical response. The following section focuses on the energy dissipation pathways in gradient PDC samples that are pyrolyzed under different temperatures as illustrated in Fig. 7.

Effect of Pyrolysis Temperature on Energy Dissipation Pathways

In this set of calculations, four gradient ceramic-polymer samples with thickness of 20 mm are considered as shown in Fig. 7. It should be noted that the two samples processed under 873 K and 1073 K have undecomposed polymer phase in the middle of the plate. When the pyrolysis temperature increases to 1273 K, the pure polymer phase no longer exists. Instead, the fully converted ceramic phase starts to emerge from the outer surface of the sample. The change of phase composition results in different energy dissipation mechanisms. It can be seen from Fig. 14 that a higher pyrolysis temperature can lead to an earlier and higher kinetic energy jump. This corresponds to a more brittle material response as a greater amount of strain energy is released. As shown in Fig. 15, debris shattering is observed in the gradient sample with a pyrolysis temperature of 1673 K. This is because insufficient residual polymer phase is available to "glue" the

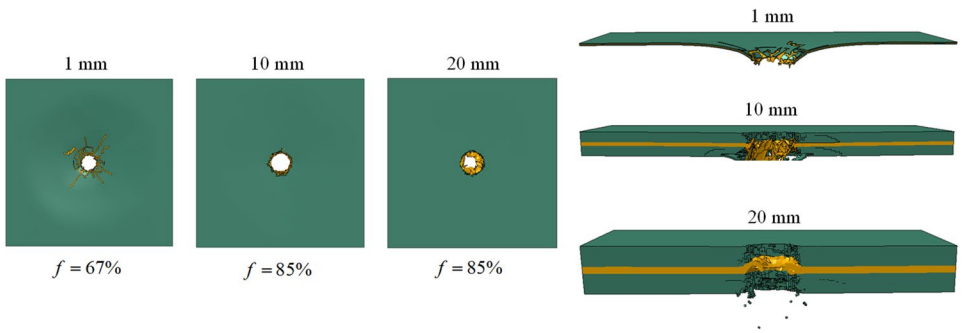

Fig. 13 Fracture patterns of ceramic-polymer composites in the contact plane and thickness plane

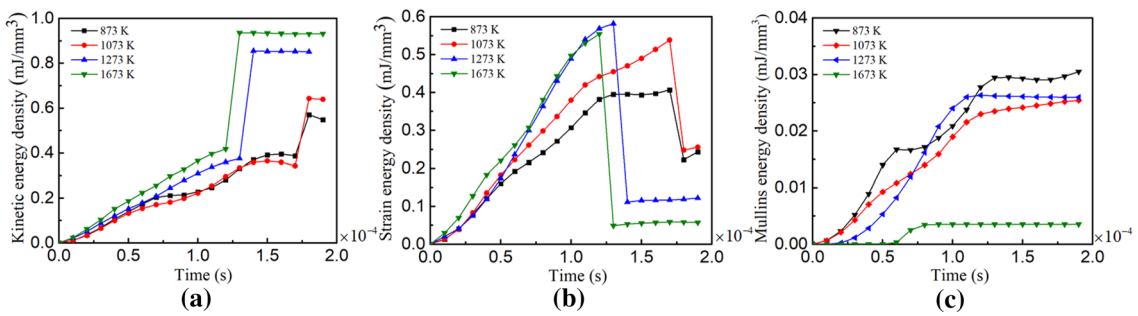

Fig. 14 Comparison of **a** kinetic energy density, **b** strain energy density and **c** Mullins energy density in gradient samples

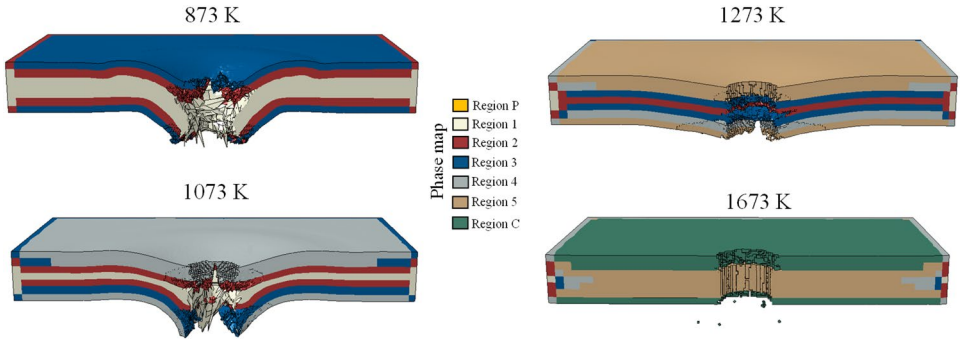

Fig. 15 Fracture patterns in gradient samples pyrolyzed under 873 K, 1073 K, 1273 K and 1673 K, respectively. Middle cross-section is selected

fractured pieces without shattering. As shown in Fig. 14c, the energy dissipation due to the Mullins effect at 1673 K is the lowest among all the cases. The strain energy released from the plate is largely transferred to the kinetic energy of the debris, as indicated in Fig. 14a. It should be noted that the lowest pyrolysis temperature of 873 K, although leading to a more ductile material response and improved structural integrity due to the enhanced Mullin's effect, can compromise the material's strength. As shown in Fig. 14b, the gradient sample pyrolyzed at 1073 K exhibits high strength that is comparable to samples pyrolyzed at 1273 K and 1673 K. At the same time, it maintains the good properties that are observed at 873 K, such as excellent structural integrity and additional load bearing capacity when fracture initiates. We further compare the performance of the 20 mm gradient sample pyrolyzed at 1073 K (Sample a) with the idealized laminate samples with thickness of 1 mm (Sample b) and 20 mm (Sample c) as discussed in "Effect of Plate Thickness and Ceramic Fraction on Energy Dissipation Pathways" section. The results shown in Fig. 16 indicate that the gradient sample can better mitigate the impact load than the idealized laminate sample (Fig. 13) when the thickness is 20 mm. The intermediate phases, especially those with higher polymer fraction in the middle of the sample, can promote energy dissipation through the Mullin's effect. It is also noted from Fig. 16b that the gradient sample exhibits the highest residual strain energy density when ball penetration occurs. This proves the earlier hypothesis that replacing the pure ceramic phase with a gradient polymer-to-ceramic phase can improve the energy absorption and structural integrity of a thick composite plate.

The above discussion points out that an effective way to improve the structure integrity of a ceramic-polymer composite without sacrificing too much of its strength is to create a gradient composition, in which the brittle ceramic phase is bonded by a ductile polymer or an intermediate phase. The polymer-derived ceramics (PDC) route, which provides great flexibility in phase composition control, is especially useful for fabricating thick composite plates with complex internal features where traditional laminating processes are not applicable.

Summary

A computational framework was developed to investigate the energy dissipation mechanisms in polymer derived ceramic composites and their effect on mechanical response. Calculations concern both idealized and gradient ceramic-polymer composites that are pyrolyzed from PMHS/DVB preceramic polymers with systematically varied pyrolysis temperatures. It was found that debris shattering in a fully converted ceramic plate upon impact loading is due to its limited energy dissipation pathways. This is because, in the

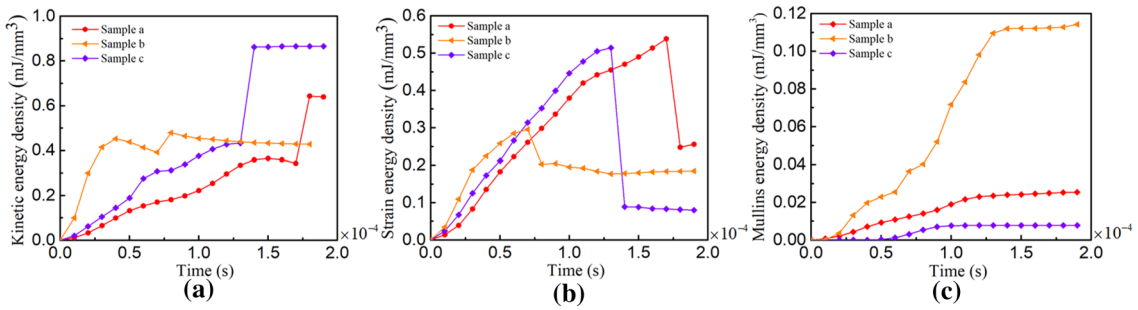

Fig. 16 Comparison of the **a** kinetic energy density, **b** strain energy density and **c** Mullins energy density in the 20 mm gradient sample (Sample **a**), 1 mm idealized laminate sample (Sample **b**) and 20 mm idealized sample (Sample **c**)

absence of inelastic and viscous deformation, the kinetic energy from the impactor cannot be fully accommodated by the plate through fracture surface formation. Therefore, the remaining kinetic energy has to be dissipated through the flying debris. Inclusion of the polymer phase to the existing ceramic plate can redistribute the kinetic energy by creating new energy dissipation mechanisms. The analysis reveals that a much larger fracture-impacted area is observed when the polymer phase is introduced. The changed fracture pattern not only leads to higher fracture energy dissipation, but also prevents debris shattering due to the combined Mullins effect and ligament bridging effect. It was also found that the gradient polymer-ceramic composite, which is fabricated through the polymer-derived ceramic (PDC) route, can provide additional flexibility in energy dissipation pathway control and property tailoring. Careful selection of the pyrolysis temperature can yield gradient composition that leads to improved structural integrity without sacrificing the material strength.

The computational work developed here can be extended to other PDC configurations that are pyrolyzed under arbitrary heating–cooling conditions. Building the linkage among the process physics, material response, and key processing parameters can provide more direct guidance for design and manufacturing of ceramic-polymer composites with tailored properties. The approach to fabricating gradient PDC composites is especially useful for structures with complex geometries where traditional polymer laminate technology is not applicable.

Acknowledgements The authors acknowledge the support from NH BioMade Project that is provided by the National Science Foundation's Research Infrastructure Improvement Award # 1757371, as well as the start-up funds from Thayer School of Engineering at Dartmouth College.

Funding Funding was provided by National Science Foundation (Grant Number 1757371) and Thayer School of Engineering at Dartmouth College (Start-up funding).

References

1. Colombo P, Mera G, Riedel R, Sorarù GD (2010) Polymer-derived ceramics: 40 years of research and innovation in advanced ceramics. J Am Ceram Soc 93(7):1805–1837
2. Mitchell T, Lagerlöf KP (1985) Dislocations in ceramics. Mater Sci Technol 1:944–949
3. Osnes K, Holmen JK, Hopperstad OS, Børvik T (2019) Fracture and fragmentation of blast-loaded laminated glass: an experimental and numerical study. Int J Impact Eng 132:103334
4. Yadav S, Ravichandran G (2003) Penetration resistance of laminated ceramic/polymer structures. Int J Impact Eng 28(5):557–574
5. Tan G, Yu Q, Liu Z, Wang X, Zhang M, Liu Y, Zhang Z, Ritchie RO (2021) Compression fatigue properties and damage mechanisms of a bioinspired nacre-like ceramic-polymer composite. Scr Mater 203:114089
6. Grujicic M, Ramaswami S, Snipes J (2016) Nacre-like ceramic/polymer laminated composite for use in body-armor applications. AIMS Mater Sci 3:83–113
7. Eckel ZC, Zhou C, Martin JH, Jacobsen AJ, Carter WB, Schaedler TA (2016) Additive manufacturing of polymer-derived ceramics. Science 351(6268):58–62
8. Kulkarni A, Sorarù GD, Pearce JM (2020) Polymer-derived SiOC replica of material extrusion-based 3-D printed plastics. Addit Manuf 32:100988
9. Konstantinou G, Kakkava E, Hagelüken L, Sasikumar PVW, Wang J, Makowska MG, Blugan G, Nianias N, Marone F, Van Swygenhoven H (2020) Additive micro-manufacturing of crack-free PDCs by two-photon polymerization of a single, low-shrinkage preceramic resin. Addit Manuf 35:101343
10. Jambe B, Marchand-Brynaert J, Devaux J (1995) Thermal degradation of poly(methyl-n-hexylsilylene). J Polym Sci A 33(8):1283–1292
11. Francis A (2018) Progress in polymer-derived functional silicon-based ceramic composites for biomedical and engineering applications. Mater Res Express 5(6):062003
12. Bernard S, Fiaty K, Cornu D, Miele P, Laurent P (2006) Kinetic modeling of the polymer-derived ceramics route: investigation of the thermal decomposition kinetics of poly [B-(methylamino) borazine] precursors into boron nitride. J Phys Chem B 110(18):9048–9060
13. Ma C, Li Y (2022) Modeling of phase transition in fabrication of polymer-derived ceramics (PDCs). Int J Comput Mater Sci Eng 11(02):2150032
14. Stabler C, Reitz A, Stein P, Albert B, Riedel R, Ionescu E (2018) Thermal properties of SiOC glasses and glass ceramics at elevated temperatures. Materials 11(2):279
15. Contact constraint enforcement methods in Abaqus/Explicit, https://abaqus-docs.mit.edu/2017/English/SIMACAEITNRefMap/simaitn-c-expcontactconstraints.htm.
16. Diani J, Fayolle B, Gilormini P (2009) A review on the Mullins effect. Eur Polymer J 45(3):601–612
17. Ma C, Ji T, Robertson CG, Rajeshbabu R, Zhu J, Dong Y (2017) Molecular insight into the Mullins effect: irreversible disentanglement of polymer chains revealed by molecular dynamics simulations. Phys Chem Chem Phys 19(29):19468–19477
18. Hohenberger TW, Windslow RJ, Pugno NM, Busfield JJC (2019) A constitutive model for both low and high strain nonlinearities in highly filled elastomers and implementation with user-defined material subroutines in ABAQUS. Rubber Chem Technol 92(4):653–686
19. Hanson DE, Hawley M, Houlton R, Chitanvis K, Rae P, Orler EB, Wrobleski DA (2005) Stress softening experiments in silica-filled polydimethylsiloxane provide insight into a mechanism for the Mullins effect. Polymer 46(24):10989–10995
20. Volokh KY (2007) Hyperelasticity with softening for modeling materials failure. J Mech Phys Solids 55(10):2237–2264
21. Kim TK, Kim JK, Jeong OC (2011) Measurement of nonlinear mechanical properties of PDMS elastomer. Microelectron Eng 88(8):1982–1985
22. Shahriari M, Saeidi Googarchin H (2020) Numerical investigation of the impact fracture performance of a composite laminated windshield considering the Park-Paulinho-Roesler cohesive zone model. Compos Struct 249:112568
23. Moysan C, Riedel R, Harshe R, Rouxel T, Augereau F (2007) Mechanical characterization of a polysiloxane-derived SiOC glass. J Eur Ceram Soc 27(1):397–403
24. Vashisth A, Khatri S, Hahn SH, Zhang W, Van Duin ACT, Naraghi M (2019) Mechanical size effects of amorphous

polymer-derived ceramics at the nanoscale: experiments and ReaxFF simulations. Nanoscale 11(15):7447–7456
25. To T, Stabler C, Ionescu E, Riedel R, Célarié F, Rouxel T (2020) Elastic properties and fracture toughness of SiOC-based glass-ceramic nanocomposites. J Am Ceram Soc 103(1):491–499
26. Shahriari M, Googarchin HS (2020) Numerical investigation of the impact fracture performance of a composite laminated windshield considering the Park-Paulinho-Roesler cohesive zone model. Compos Struct 249:112568